

Controlling shedding characteristics of condensate drops using electrowetting

Ranabir Dey,¹ Jander Gilbers,¹ Davood Baratian,¹ Harmen Hoek,¹ Dirk van den Ende,¹ and Frieder Mugele^{1, a)}
*Physics of Complex Fluids, MESA+ Institute for Nanotechnology, University of Twente, PO Box 217,
 7500 AE Enschede, The Netherlands*

We show here that ac electrowetting (ac-EW) with structured electrodes can be used to control the gravity-driven shedding radius and shedding rate of drops condensing onto flat hydrophobic surfaces. For straight interdigitated electrodes the ac-EW-induced reduction of effective contact angle hysteresis results in smaller gravity-driven shedding radius, which, coupled with the enhanced growth due to coalescence under EW, result in increased shedding rate. Interestingly, we further show that the condensate droplet pattern under EW can be controlled, and the coalescence can be further enhanced, by judicious design of the interdigitated electrodes with zigzag edges. Such enhanced coalescence in conjunction with the electrically-induced trapping effect due to the electrode geometry result in larger shedding radius of the condensate drops, but lower shedding rate. However, the shedding radius and the shedding rate can be further optimized by applying the electrical voltage in a periodic manner. We finally provide a conservative estimate of the average condensate removal rate for different ac-EW induced shedding characteristics, and highlight the advantages of ac-EW-controlled condensate shedding.

Dropwise condensation is fundamentally important in a wide range of technologies like water-harvesting systems¹, desalination systems², and heat exchangers³. The effectiveness of all these technologies is intrinsically dependent on the efficient shedding of the condensate drops from the condensing surface. The continuous drop shedding exposes bare surface for renewed nucleation and growth of the condensate drops culminating in efficient vapour-to-liquid phase change and enhanced heat transfer⁴. To this end, the enhanced mobility and shedding of condensate drops have been successfully studied on superhydrophobic nanostructured surfaces^{5–8}, wettability-patterned surfaces⁹, liquid impregnated textured surfaces^{10,11}, and biomimetic surfaces¹². However, all these approaches towards enhancing droplet mobility are passive in nature, relying solely on the topographical and/or chemical patterning of the underlying condensing surface. As an alternative, very recently we have demonstrated that an alternating (ac) electric field in an electrowetting (EW) configuration with structured electrodes actively controls the mobility of condensate drops on homogeneous hydrophobic surfaces¹³. The growth of the condensate drops under EW is characterized by their migration to the size-dependent locations of the minima in the corresponding electrostatic energy landscapes and enhanced coalescence¹³. The use of EW to control condensate droplet pattern (breath figures) evolution is— to our knowledge— a completely new approach, which goes beyond the aforementioned passive approaches. In this regard, a detailed study of the final gravity-driven shedding characteristics of the condensate drops under ac-EW is still necessary. Such a study is essential to first understand the effect of ac-EW on the shedding of the condensate drops, and thereby devise recipes for effective implementation of EW for technological applications involving dropwise condensation.

In this letter, we demonstrate that the gravity-driven shedding characteristics of condensate drops can be indeed controlled using ac-EW with structured electrodes. We show that under ac-EW with straight interdigitated electrodes, the underlying reduction in effective contact angle hysteresis and the enhanced coalescence-dominated growth of the condensate drops result in smaller shedding radius and increased shedding rate as compared to the classical no EW case. Interestingly, we also show that the shedding characteristics under ac-EW can be further altered using interdigitated electrodes with zigzag edges. In this case, the mobility of condensate drops in non-uniform electric fields and the electrical trapping effect result in larger shedding radius and lower shedding rate; however, the overall condensate removal rate increases. Finally, we also demonstrate that the shedding of condensate is further enhanced by applying the electrical voltage in a periodic manner instead of continuously.

The condensation experiments are performed using a setup identical to that used in our previous study¹³. The condensing substrate consists of interdigitated ITO electrodes fabricated on a glass substrate, which is coated with a hydrophobic dielectric polymer film— 2 μm thick Parylene C layer topped with an ultrathin layer of Cytop (Fig. 1(a)). For the straight interdigitated electrodes (Fig. 1(b)(i)) the width of both the electrodes (red) and the gaps (intermediate orange) is 200 μm ; for the zigzag interdigitated electrodes (Fig. 1(b)(ii)) the base and the apex of each triangular element for both electrodes and gaps are 250 μm and 50 μm wide respectively, while the distance l between the consecutive triangular elements is varied from 500 μm to 3000 μm to create different electrode designs. For EW, an ac voltage with a frequency of $f = 1$ kHz and a maximum magnitude of 150 V U_{rms} is applied across the electrodes (Fig. 1(a), (b)). Thereafter, a stream of vapour-air mixture at a flow rate of 3.6 l/min and a temperature of 41.8 $^{\circ}\text{C}$ is passed through a condensation chamber, in which the substrate is maintained at a temperature of 11.5 $^{\circ}\text{C}$. Condensation experiments are performed without EW ($U_{rms} = 0$ V), and under ac-

^{a)} e-mail: f.mugele@utwente.nl

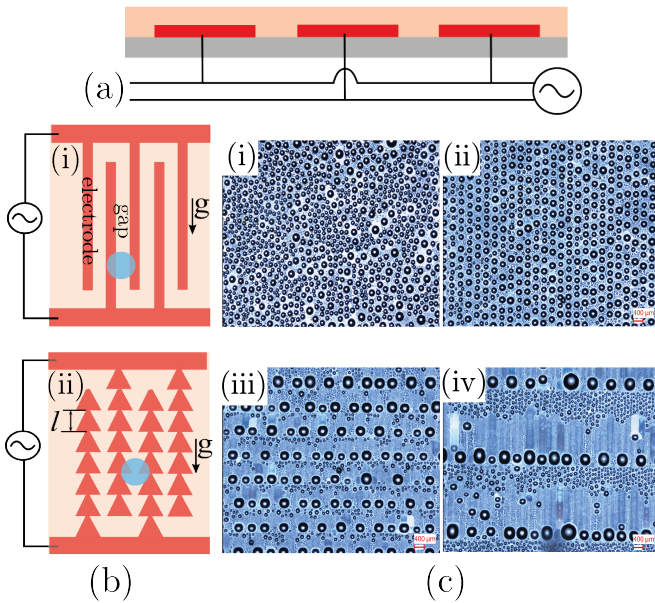


FIG. 1. (a) Schematic of the substrate used for the condensation experiments. The substrate consists of transparent interdigitated ITO electrodes (red) patterned on a glass substrate (gray), which is coated with a hydrophobic dielectric film (orange). (b) Schematics showing the underlying interdigitated electrode (electrode-gap) designs– (i) straight interdigitated electrodes, (ii) interdigitated electrodes with zigzag edges; the distance l between the consecutive triangular elements is varied to create different electrode designs. (c) Comparison between condensate droplet patterns (at approximately the same time instant) without EW (i) and with EW ($U_{rms} = 150$ V; $f = 1$ kHz) on substrates with different electrode designs– (ii) straight interdigitated electrodes, (iii) zigzag interdigitated electrodes with $l = 1000$ μm and (iv) $l = 3000$ μm . Gravity points from top to bottom along the electrodes as shown in (b).

EW by applying different magnitudes of U_{rms} first using straight interdigitated electrodes and then using zigzag interdigitated electrodes with $l = 500$ μm , 1000 μm , and 3000 μm . The condensation process, including the shedding events, is monitored using a high resolution camera.

In times prior to shedding in absence of EW ($U_{rms} = 0$ V), the condensate drops are apparently randomly distributed with smaller average sizes (Fig. 1(c)(i); also see Movie S1 in the supplementary material). However, in the build up to shedding under ac-EW with straight interdigitated electrodes, the condensate drops having diameters comparable to or greater than the gap width migrate to, and remain aligned along, the corresponding electrostatic energy minima locations at the gap centres (Fig. 1(c)(ii); also see Movie S2 in the supplementary material). Formation of such condensate droplet pattern is in accordance with our earlier study on breath figure evolution under ac-EW¹³. The underlying fact that the location and the coalescence induced growth of

the condensate drops under EW can be controlled simply by tuning the electric field (via electrode design) is exploited here using the zigzag interdigitated electrodes towards altering the final shedding characteristics. The zigzag electrode geometry results in increasing electric field strength along the converging gap geometry. Consequently, in this case the condensate drops move in the direction of the increasing electric field magnitude. Eventually, the droplets accumulate to form large droplets at the apices of the triangular gap elements due to the electrical trapping effect at these locations (see the schematic in Fig. 1(b)(ii)). Hence, the condensate droplet pattern under EW with zigzag interdigitated electrodes also has a periodicity along the direction parallel to the electrodes which is dependent on l (compare Fig. 1(c)(ii) and Fig. 1(c)(iii) or (iv)). Larger l results in larger sizes of the trapped condensate droplets, due to the collection of condensate drops over larger regions, and larger periodicity (smaller spatial frequency) of the droplet pattern along the direction parallel to the electrodes (compare Fig. 1(c)(iii) and Fig. 1(c)(iv); also see Movie S3, Movie S4 and Movie S5 in the supplementary material for condensate droplet pattern evolution corresponding to $l = 1000$ μm , 3000 μm , and 500 μm respectively). Interestingly, the above described mobility and growth of the condensate drops under different ac-EW conditions alter the final gravity-driven shedding characteristics from those classically observed without EW.

The final gravity-driven shedding characteristics are quantified here by the average shedding radius $\langle R_{sh} \rangle$ of the condensate drops, and the average shedding rate $\langle f_{sh} \rangle$. The shedding radius R_{sh} is defined as the radius of a condensate drop at which it just begins to slide on the condensing surface, as evaluated using an image analysis procedure (Fig. 2(a); for the image analysis procedure see Sec. S1 in the supplementary material); $\langle R_{sh} \rangle$ represents the average value of R_{sh} evaluated using on an average 40 shedding events corresponding to a particular EW condition. $\langle f_{sh} \rangle$ is evaluated simply by dividing the total number of recorded shedding events with the total time required for these shedding events starting from the opening of the vapour valve for the initiation of the condensation process. Fig. 2(b) clearly shows that $\langle R_{sh} \rangle$ progressively reduces under ac-EW, with straight interdigitated electrodes, with increasing magnitude of U_{rms} ; $\langle R_{sh} \rangle$ for $U_{rms} = 150$ V is approximately 50% smaller than that observed without EW. It must be first noted here that in absence of EW a condensate drop begins to shed under gravity only when the weight of the drop overcomes the inherent surface hysteresis force, as valid for the classical problem of gravity-driven drop mobilization on a vertical substrate¹⁴. Accordingly, $\langle R_{sh} \rangle$ can be estimated as $\langle R_{sh} \rangle \approx \sqrt{\frac{3}{\pi}} \lambda_c (\Delta \cos \theta)^{1/2}$, where $\lambda_c = \sqrt{\frac{\gamma}{\rho g}}$ is the capillary length, γ and ρ are the surface tension and the density of water respectively, and $\Delta \cos \theta$ is the difference between the cosines of the receding and advancing contact angles of water drops on the

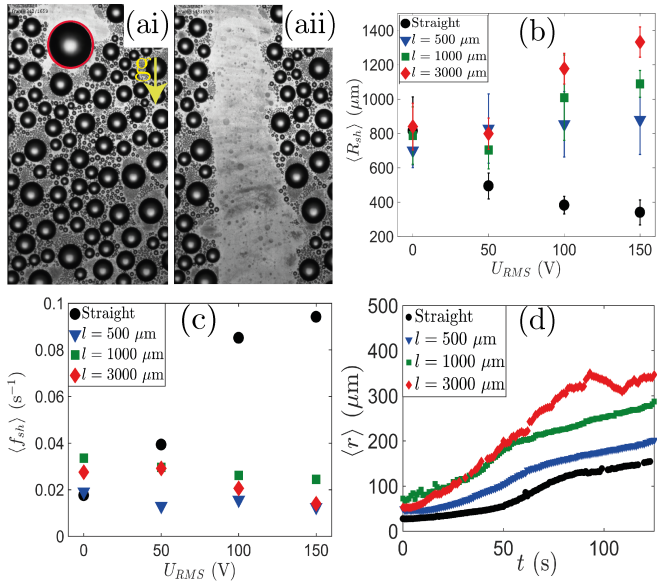


FIG. 2. (ai) Representative image of a condensate drop (outlined in red) an instant (a frame) before gravity assisted shedding from the surface. The radius of the drop at this instant is defined as the shedding radius R_{sh} . (aai) The consequent frame showing the clearing of the surface due to the shedding of the same droplet; the shedding droplet sweeps away all the droplets in its path. (b) Variations of the average droplet shedding radius $\langle R_{sh} \rangle$ with the applied voltage U_{rms} for different electrode designs, i.e. straight interdigitated electrodes (Fig. 1(bi)) and zigzag interdigitated electrodes with different values of l (Fig. 1(bii)). (c) Variations of the average shedding rate $\langle f_{sh} \rangle$ with U_{rms} for the different electrode designs. (d) Growth of the area-weighted mean radius $\langle r \rangle$ of the condensate drops in the breath figure under ac-EW ($U_{rms} = 150$ V) with different electrode designs.

condensing surface which gives a measure of the involved contact angle hysteresis (CAH) (see Sec. S2 in the supplementary material for details). In regard to CAH, it is now well established that generally under ac-EW in air the effective CAH gradually decreases with increasing AC voltage^{15–17}. This reduction in CAH is due to the oscillatory electrical force induced depinning of the three-phase contact line from the random surface heterogeneities, and can be expressed as $\Delta \cos \theta(U_{rms}) \approx \Delta \cos \theta_0 - \beta U_{rms}^2$, where $\Delta \cos \theta_0$ is the value of $\Delta \cos \theta$ for $U_{rms} = 0$ V, and β is a prefactor dependent on the electrical permittivity of the hydrophobic dielectric film, its thickness and γ ^{15,16}. It is such ac-EW induced reduction in CAH of the condensate drops on the condensing surface (see Sec. S2 in the supplementary material) that results in the observed reduction of $\langle R_{sh} \rangle$ with U_{rms} for ac-EW with straight interdigitated electrodes; hence, the voltage dependent shedding radius can be estimated as $\langle R_{sh} \rangle \approx \sqrt{\frac{3}{\pi} \lambda_c [\Delta \cos \theta_0 - \beta U_{rms}^2]^{1/2}}$. Furthermore, the gradually decreasing value of $\langle R_{sh} \rangle$, coupled with the enhanced coalescence induced droplet growth under EW,

results in the corresponding increasing value of $\langle f_{sh} \rangle$ with increasing U_{rms} (Fig. 2(c)). However, under ac-EW with zigzag interdigitated electrodes, $\langle R_{sh} \rangle$ increases, instead of reducing, with increasing value of U_{rms} (Fig. 2(b)). This is because in order to shed under ac-EW with zigzag interdigitated electrodes, the condensate droplet weight has to overcome an additional electrical force due to the electrode geometry induced trapping effect. So, for this case $\langle R_{sh} \rangle$ can be estimated from the relation

$$\langle R_{sh} \rangle^3 \approx \frac{3}{\pi} \lambda_c^2 (\Delta \cos \theta_0 - \beta U_{rms}^2) \langle R_{sh} \rangle + \frac{1.5}{\pi} \lambda_c^2 \beta U_{rms}^2 \Delta l_c^h \quad (1)$$

where the last term in Eq. 1 is due to the additional electrical trapping force, and Δl_c^h represents the difference between the horizontal projections of the total droplet contact line length on the zigzag electrode elements above the horizontal droplet footprint diameter and of the same below it (see Sec. S3 in the supplementary material for details). Since the electrical trapping force is $\propto U_{rms}^2$ the enhancement in $\langle R_{sh} \rangle$ with increasing U_{rms} is more pronounced for higher values of the latter (Fig. 2(b)). Furthermore, Δl_c^h in Eq. 1 is also dependent on the slope of the zigzag edges of the electrode elements, and hence, dependent on l ; Δl_c^h increases with increasing value of l (see Sec. S3 in the supplementary material). Accordingly, the electrical trapping force increases with increasing l ; consequently, $\langle R_{sh} \rangle$ increases with increasing value of l for a definite value of U_{rms} (Fig. 2(b)). It is also worth noting here that Eq. 1 provides a reasonable estimate for $\langle R_{sh} \rangle$ under ac-EW with zigzag interdigitated electrodes for moderate values of U_{rms} , on considering l as a scale for Δl_c^h ; for e.g., the experimental values of $\langle R_{sh} \rangle$ for $l = 1000 \mu\text{m}$ and $l = 3000 \mu\text{m}$, at $U_{rms} = 100$ V, are $1008 \mu\text{m}$ and $1178 \mu\text{m}$ respectively, while the corresponding values obtained by numerically solving Eq. 1 are $928 \mu\text{m}$ and $1100 \mu\text{m}$ respectively (considering $\Delta \cos \theta_0 \approx 0.15$ and $\beta \sim 6.18 \times 10^{-6}$; see Sec. S2 in the supplementary material). However, for larger values of U_{rms} , Eq. 1 underestimates the value of $\langle R_{sh} \rangle$ because CAH does not go on decreasing under ac-EW with increasing U_{rms} (as considered during formulation of Eq. 1), but stabilizes at a finite, albeit smaller, value for moderate values of U_{rms} ^{15,16}. Finally, the increasing value of $\langle R_{sh} \rangle$ due to the electrical trapping effect results in smaller values of $\langle f_{sh} \rangle$ for the zigzag interdigitated electrodes, as compared to the straight interdigitated electrodes (Fig. 2(c)).

Interestingly, the aforementioned shedding characteristics under ac-EW with zigzag interdigitated electrodes can be further altered by applying U_{rms} in a periodic manner instead of continuously. In this regard, it must be first noted that the growth rate of condensate drops increases under ac-EW with zigzag interdigitated electrodes as quantitatively demonstrated by the temporal variations of the area-weighted average radius of the condensate drops ($\langle r \rangle(t) = \Sigma r^3 / \Sigma r^2$) under different EW conditions (Fig. 2(d)). $\langle r \rangle$ increases with increasing l (Fig. 2(d)) due to the enhanced mobility and coalescence of drops over progressively larger regions of non-uniform

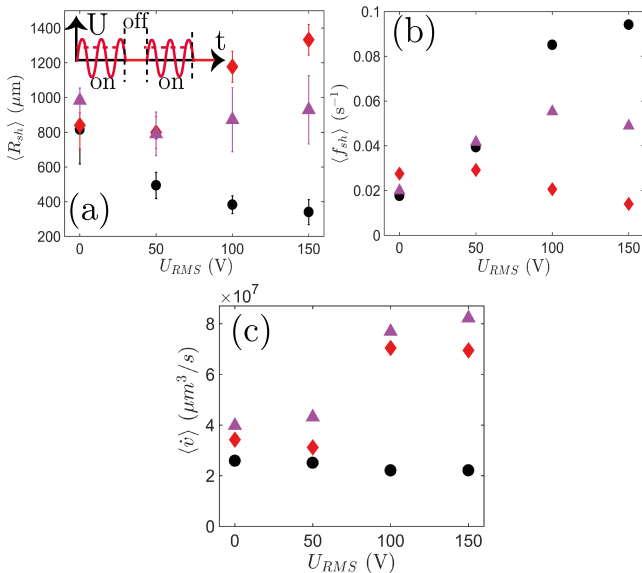


FIG. 3. (a) Variations of the average droplet shedding radius $\langle R_{sh} \rangle$ with the applied voltage U_{rms} for dropwise condensation under continuous ac-EW (circular markers: straight interdigitated electrodes; diamond markers: zigzag interdigitated electrodes with $l = 3000 \mu\text{m}$), and under periodic ac-EW (triangular markers: identical zigzag interdigitated electrodes). The periodic ac-EW is achieved by switching the applied sinusoidal voltage on (50 s) and off (10 s) in an automated manner as schematically represented in the inset. (b) Variations of the average shedding rate $\langle f_{sh} \rangle$ with U_{rms} for continuous ac-EW and periodic ac-EW. (c) Conservative estimates for the variations of the average condensate removal rate $\langle \dot{v} \rangle$ with U_{rms} for the different EW conditions. The symbols in (b) and (c) represent the identical EW conditions as defined in (a).

electric field, as can be also inferred from Fig. 1(c). Furthermore, it must be also noted here that in absence of EW, $\langle R_{sh} \rangle \sim O(\lambda_c)$. Hence, it is possible to alter the associated shedding characteristics for the zigzag interdigitated electrodes by first applying U_{rms} for a certain interval of time in order to promote the aforementioned faster growth of the condensate drops towards a radius $\sim \lambda_c$, and then by subsequently switching it off for some time in order to facilitate the gravity-driven shedding by turning off the electrical trapping effect. We demonstrate here the feasibility of this concept by applying U_{rms} in a periodic manner as shown in the inset in Fig. 3(a). Fig. 3(a) clearly shows that $\langle R_{sh} \rangle$ under ac-EW with zigzag interdigitated electrodes having $l = 3000 \mu\text{m}$ decreases under periodic ac-EW as compared to continuous ac-EW due to the intermittent switching off of the electrical trapping effect; note that the resulting value of $\langle R_{sh} \rangle$ under periodic ac-EW is comparable to that obtained without EW. However, the resulting $\langle f_{sh} \rangle$ increases (approximately 1.5 times) under periodic ac-EW as compared to that obtained without EW (Fig. 3(b)) due to the associated faster growth rate of drops (Fig.

2(d)). Finally, we provide a rough estimate of the condensate removal rate ($\langle \dot{v} \rangle \approx \frac{2}{3}\pi \langle R_{sh} \rangle^3 \times \langle f_{sh} \rangle$) corresponding to the different EW-controlled shedding characteristics (Fig. 3(c)). In this regard, $\langle \dot{v} \rangle$ remains approximately similar with increasing U_{rms} for ac-EW with straight interdigitated electrodes (Fig. 3(c)); this is because the associated reduction in $\langle R_{sh} \rangle^3$ (Fig. 2(b)) nullifies the increase in $\langle f_{sh} \rangle$ (Fig. 2(c)). However, $\langle \dot{v} \rangle$ significantly increases (almost by a factor of 2) for ac-EW with zigzag interdigitated electrodes; specifically, the case of periodic ac-EW is relatively advantageous than continuous ac-EW (Fig. 3(c)). This is because in the case of ac-EW with zigzag interdigitated electrodes the significant increase in $\langle R_{sh} \rangle^3$ (Fig. 2(b)) dominates over the reduction in $\langle f_{sh} \rangle$ (Fig. 2(c)) resulting in the significant enhancement in the overall condensate removal rate. It must be noted here that a quantitatively accurate estimate of $\langle \dot{v} \rangle$ must also include the volume of all the condensate drops swept away by the shedding drop, and hence, requires a separate experimental measurement procedure. However, the estimate for $\langle \dot{v} \rangle$ provided in Fig. 3(c) gives a working idea about the relative condensate removal rates for the different ac-EW induced shedding characteristics.

In summary, we have shown that the shedding characteristics of condensate drops can be controlled using ac-EW with structured electrodes. The combination of ac-EW induced reduction of CAH, mobility of drops in non-uniform electric fields, and the electrical trapping effect are the main ingredients which when judiciously combined results in significantly enhanced shedding of condensate, as compared to the classical no EW case. It must be also noted here that the methodologies for implementing ac-EW towards achieving enhanced condensate shedding are not restricted to only those demonstrated here; different electrode designs and different electrical voltage waveforms can be still conceived for further optimization of the shedding characteristics. We hope that this work will trigger further research in that direction. Finally, the observed ac-EW induced shedding characteristics will definitely alter the associated heat transfer characteristics from those classically observed. However, rigorous experiments involving simultaneous measurements of heat transfer characteristics and shedding characteristics under different ac-EW conditions are necessary to unambiguously identify the ac-EW conditions conducive for enhanced heat transfer during dropwise condensation. Such an endeavour can definitely be the scope of future research work.

ACKNOWLEDGMENTS

We thank Daniel Wijnperle for his immense help with the preparation of the condensation substrates. We acknowledge financial support by the Dutch Technology Foundation STW, which is part of the Netherlands Organization for Scientific Research (NWO), and the VICI program (grant 11380).

- ¹D. Milani, A. Abbas, A. Vassallo, M. Chiesa, and D. Al Bakri, *Chemical Engineering Science* **66**, 2491 (2011).
- ²A. D. Khawaji, I. K. Kutubkhanah, and J.-M. Wie, *Desalination* **221**, 47 (2008).
- ³M.-H. Kim and C. W. Bullard, *International Journal of Refrigeration* **25**, 924 (2002).
- ⁴J. Rose, *Proceedings of the Institution of Mechanical Engineers, Part A: Journal of Power and Energy* **216**, 115 (2002).
- ⁵J. B. Boreyko and C.-H. Chen, *Physical Review Letters* **103**, 184501 (2009).
- ⁶N. Miljkovic, R. Enright, and E. N. Wang, *ACS Nano* **6**, 1776 (2012).
- ⁷N. Miljkovic, R. Enright, Y. Nam, K. Lopez, N. Dou, J. Sack, and E. N. Wang, *Nano Letters* **13**, 179 (2012).
- ⁸N. Miljkovic, D. J. Preston, R. Enright, and E. N. Wang, *ACS nano* **7**, 11043 (2013).
- ⁹A. Ghosh, S. Beaini, B. J. Zhang, R. Ganguly, and C. M. Megaridis, *Langmuir* **30**, 13103 (2014).
- ¹⁰S. Anand, A. T. Paxson, R. Dhiman, J. D. Smith, and K. K. Varanasi, *ACS Nano* **6**, 10122 (2012).
- ¹¹H. Tsuchiya, M. Tenjimabayashi, T. Moriya, R. Yoshikawa, K. Sasaki, R. Togasawa, T. Yamazaki, K. Manabe, and S. Shiratori, *Langmuir* (2017).
- ¹²K.-C. Park, P. Kim, A. Grinthal, N. He, D. Fox, J. C. Weaver, and J. Aizenberg, *Nature* **531**, 78 (2016).
- ¹³D. Baratian, R. Dey, H. Hoek, D. van den Ende, and F. Mugele, *Physical Review Letters* **120**, 214502 (2018).
- ¹⁴P.-G. de Gennes, F. Brochard-Wyart, and D. Quere, *Capillarity and Wetting Phenomena: Drops, Bubbles, Pearls, Waves* (Springer New York, 2004).
- ¹⁵F. Li and F. Mugele, *Applied Physics Letters* **92**, 244108 (2008).
- ¹⁶D. t Mannetje, C. Murade, D. Van Den Ende, and F. Mugele, *Applied Physics Letters* **98**, 014102 (2011).
- ¹⁷J. Gao, N. Mendel, R. Dey, D. Baratian, and F. Mugele, *Applied Physics Letters* **112**, 203703 (2018).